JOURNAL OF MATERIALS SCIENCE 4 (1969) 223–235

# Dislocation Morphology in Graded Heterojunctions: $GaAs_{1-x}P_x$

M. S. ABRAHAMS, L. R. WEISBERG, C. J. BUIOCCHI, J. BLANC
*RCA Laboratories, Princeton, NJ 08540, USA*

*Received 4 October 1968, and in revised form 26 November*

The details of the formation, propagation, interaction, and densities of misfit dislocations are combined into a simple model quantitatively predicting dislocation densities for both abrupt and graded heterojunctions. Three key concepts are introduced: (1) misfit dislocations are segmented; (2) accordingly, they must give rise to a density of inclined dislocations, $n_I$, that propagate through the growing layer; and (3) these inclined dislocations can bend in and out of any subsequently formed misfit plane to relieve the strain, and when bent in, serve as strain-relieving misfit dislocations. Thus, the value of $n_I$ is expected to remain constant with thickness. Also, $n_I$ is predicted to vary directly with the compositional gradient at the heterojunction. It is pointed out that there are two general classes of misfit dislocations, pure-edge and mixed and that their intersections, which cause the misfit dislocations to appear to bend within their plane, can be simply classified into three general types.

Transmission electron microscopy was used for a comprehensive study of dislocations in a series of $GaAs_{1-x}P_x$ heterojunctions prepared by a vapour phase growth technique. The main features of the above model were corroborated. The value of $n_I$ was found to be constant with growth distance as postulated, and in quantitative agreement with prediction, $n_I$ decreased from $4 \times 10^7$ cm$^{-2}$ to $10^6$ cm$^{-2}$ as the compositional gradient decreased from 5% phosphorus/$\mu$m to 0.2% phosphorus/$\mu$m. Note that these values can far exceed the dislocation density of the substrates. Of particular significance, the inclined dislocations $n_I$ were found to propagate through a constant-composition region grown on top of a compositionally graded region, so that formation of the heterojunction must affect subsequently grown layers. Finally, it is shown that the misfit dislocations are, indeed, a combination of pure-edge and mixed, and all three postulated general interactions between these dislocations are shown to occur.

## 1. Introduction

The formation of a boundary between two dissimilar materials, i.e. a heterojunction, has been the subject of considerable interest concerning its electrical characteristics, which depend upon whether the boundary is abrupt [1] or graded [2, 3]. However, much less attention has been given to the lattice defects, such as dislocations, at and through such heterojunctions. This latter subject has recently become of increasing importance, since, for example, a wide variety of structures and devices are being prepared in the $GaAs_{1-x}P_x$ alloy system [4-7]. In these cases, the alloy is typically grown on a GaAs substrate, so that a heterojunction inevitably forms.

It is well known that the lattice mismatch at a boundary between two materials will cause "misfit" dislocations to form because of the change in the lattice parameter at the boundary [8]. This has recently been demonstrated for p-n junctions in GaAs [9], and also for heterojunctions in the $Ga_xIn_{1-x}Sb$ system [10]. In the present research details concerning the formation, densities, propagation, and interactions of misfit dislocations, especially in a graded heterojunction, are incorporated into a simple quantitative model.

This model allows the tangles of dislocations observed at heterojunctions to be understood in detail. The main features of the model are substantiated by a comprehensive study of these misfit dislocations by transmission electron microscopy in the $GaAs_{1-x}P_x$ system. It will be shown that the density of misfit dislocations can be surprisingly high ($10^5$ to $10^8$ cm$^{-2}$), and therefore might have a profound effect on the electrical characteristic of p-n junctions formed at or even near the heterojunction.

The use of transmission electron microscopy here is important since many of the dislocations observed in the $GaAs_{1-x}P_x$ alloys, especially the small segmented dislocations discussed later, may not be revealed by etchants used for GaAs alone, such as the A-B etchant [5, 11]. Furthermore, at the high dislocation densities seen here, X-ray topographic techniques do not provide sufficient resolution.

When misfit dislocations form at a heterojunction, most, but not all, of the strain is relieved in the process. It has been shown that residual strain still exists at a misfit plane [12, 13]. Furthermore, additional strain can arise due to differential thermal contraction after formation of the heterojunction. The relationship between strain and the dislocation morphology will be the subject of a forthcoming paper, and is ignored here.

## 2. Model of Dislocation Formation, Propagation and Interaction

### 2.1. Dislocations in a Single Misfit Plane

The linear density, $n_L$, per cm of misfit dislocations emerging from the edge of a misfit plane at which there is an abrupt change in lattice constant, $\Delta\lambda$, is given by [8]:

$$n_L = \frac{\Delta\lambda}{\lambda^2} \qquad (1)$$

where $\lambda$ is the mean lattice parameter above and below the misfit plane. The value of $n_L$ can be quite large. For example, the very small change in lattice parameters between Te-doped and Zn-doped GaAs can give rise to a value of $n_L$ of $10^3$ cm$^{-1}$ at a p-n junction in GaAs [9]. In the case of GaAs grown in the [100] direction, there would be two sets of orthogonal misfit dislocations, each in the (100) plane, and parallel to the [011] and [01$\bar{1}$] directions.

In deriving equation 1, there is no assumption made concerning the length of the dislocations formed. In an ideal crystal, the dislocation would be continuous from one edge of the crystal to the other. However, ideal conditions are not maintained during crystal growth, since growth typically occurs by a heterogeneous nucleation and island growth process. As a result, one would expect the dislocations to be segmented and would appear as shown in fig. 1. This segmentation will have further effects as discussed below. Although this segmentation would not change the value of $n_L$, the number per unit area of *segmented* misfit dislocations, $n_S$, lying in the misfit plane would be increased from $2n_L$ to:

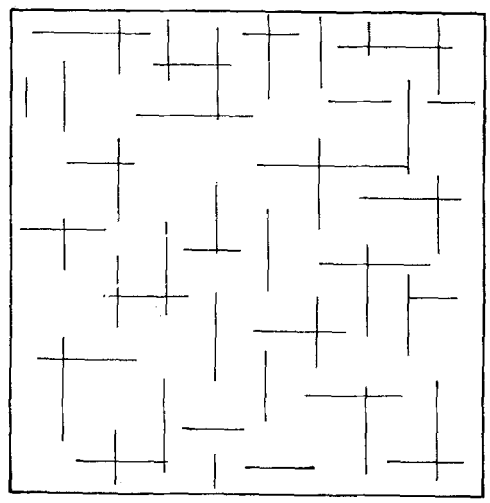

*Figure 1* Schematic representation of misfit dislocations formed in a plane of misfit due to a change in lattice constant.

$$n_S = 2n_L/L_{avg} \qquad (2)$$

where $L_{avg}$ is the average total length of a dislocation.

The assumption that misfit dislocations are segmented is a key concept in this paper. As a corollary since dislocations cannot end within a crystal, they must bend upwards and propagate through the growing crystal. This leads to a second key assumption, namely that the formation of a set of $n_S = 2n_L/L_{avg}$ segmented dislocations in a misfit plane will give rise to a set of inclined dislocations, $n_I$, with a density per cm$^2$ threading the plane of growth of:

$$n_I = 4n_L/L_{avg}\,. \qquad (3)$$

Here it is assumed that there are two inclined dislocations for each mismatch dislocation.

Evidence will be shown later of the existence of this set of $n_I$ inclined dislocations.

One can express the value of $L_{avg}$ as a multiple, $m$, of the distance between the misfit dislocations as $L_{avg} = m/n_L$. Then equation 3 reduces to

$$n_I = 4n_L^2/m \,. \tag{4}$$

Thus, a quadratic relation exists between $n_I$ and $n_L$ for a single misfit plane.

## 2.2. Dislocations in Multiple Misfit Planes

Consider that several misfit planes are formed during the growth of a crystal due to several abrupt changes in lattice constant. For simplicity, we assume that the change in lattice constant at each plane is identical, and that the planes are spaced equidistantly, a distance $\Delta X$ apart. We then calculate the total dislocation densities.

We can no longer express the total number of misfit dislocations emerging from the multiple misfit planes in terms of a linear density $n_L$, which refers to only a single misfit plane. Instead, one must introduce the quantity $n_A$ to represent the total number of misfit dislocations per unit *area* emerging at several planes from the side of the crystal. In the special case assumed above, there are a total of $(1/\Delta X)$ misfit planes per cm of crystal growth, and each misfit plane will contain $n_L$ misfit dislocations per cm of crystal width. It can be seen that:

$$n_A = \frac{n_L}{\Delta X} = \frac{1}{\lambda^2}\frac{\Delta\lambda}{\Delta X}. \tag{5}$$

Similarly, the total number of segmented dislocations per unit *volume* will be $n_s = 2n_A/L_{avg}$.

We next consider what the density of inclined dislocations, $n_I$, will be. In general, two possibilities exist, as indicated schematically in fig. 2. In the first case, according to equation 4 each misfit plane will give rise to $n_I = 4n_L^2/m$ inclined dislocations, and $n_I$ will continually increase as the crystal grows, as indicated in fig. 2a. Thus, in a distance $d$ of crystal growth, there will be a total of $n_I = (d/\Delta X)\ (4n_L^2/m)$ inclined dislocations.

In the second case (fig. 2b), instead of new misfit dislocations forming at each new misfit plane, when the inclined dislocations reach the misfit plane, they bend over into the misfit plane to relieve the strain. This is energetically more favourable since no new dislocations need be formed and the total dislocation density is lower.

Another key concept in this paper is that this second case predominates so that once there are sufficient numbers of inclined dislocations formed in the first or first few misfit planes to relieve subsequent strains, no new misfit dislocations will be formed. Accordingly, the *density*

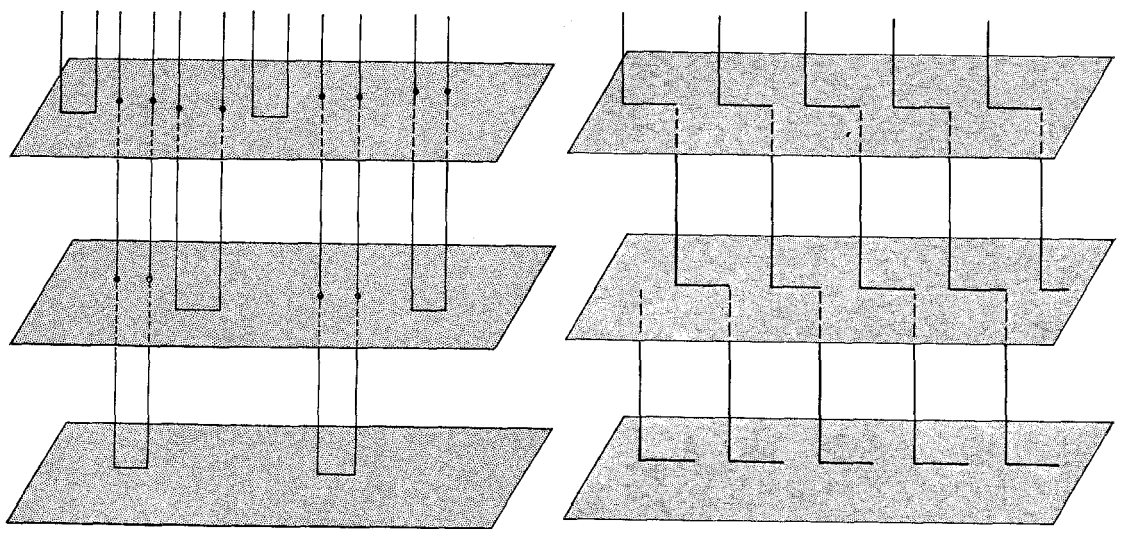

(a) (b)

*Figure 2* Simplified schematic illustration of the propagation of dislocations through multiple misfit planes: (a) new misfit dislocations originate at each misfit plane leading to increase in density of inclined dislocations with distance of growth; (b) initial misfit dislocations bend in and out of successive misfit planes leading to a constant density of inclined dislocations with distance of growth.

*of inclined dislocations will then remain constant during growth.* In this special case, there would be a total of only $n_I = 2n_L^2/m$, independent of the amount of crystal grown. Experimental support for this result will be given later.

### 2.3. Dislocations in a Graded Region

When the lattice constant changes at a uniform rate during crystal growth the concept of a linear dislocation density $n_L$ becomes useless, and one considers instead the quantity $n_A$, which is the number of dislocations per cm$^2$ emerging from the sides of the crystal. Equation 5 will still hold, but the quantity $n_L$ is ignored. Here we assume that these dislocations emerging from the sides of the crystal are uniformly distributed, and this is borne out experimentally (see fig. 10).

If we assume that the change in lattice parameter occurs due to a change in composition $\Delta C$ of the crystal during growth, and if $\Delta C$ is linearly related to $\Delta\lambda$ in a system with end values of $\lambda_A$ and $\lambda_B$ (i.e. Vegard's law applies for at least the composition range of interest, then $\Delta C = 100\ \Delta\lambda/(\lambda_A - \lambda_B)$), where $\Delta C$ is expressed in terms of the percentage of the added constituent, and

$$n_A = \frac{(\lambda_A - \lambda_B)}{\lambda^2}\left(\frac{\Delta C}{\Delta X}\right). \tag{6}$$

In any distance $\Delta X$ in the crystal, the total number of *segmented* dislocations per unit *volume* will be, in analogy to equation 2

$$n_S = 2n_A/L_{avg}. \tag{7}$$

Concerning the density of inclined dislocations $n_I$, as before we can let the number formed $n_I = 2n_S$. However, as discussed in section 2.2. above, they will form only until a steady-state condition is reached in which their density is sufficient to produce sufficient misfit dislocations in subsequent regions of growth to relieve strains. A moment's thought will show that this steady-state condition will be realized after the crystal has grown a distance equal to the average distance between dislocations, $n_A^{-1/2}$. Then the density of inclined dislocations $n_I$ will remain constant, and equal in value to:

$$n_I = n_S n_A^{-1/2} = 2n_A^{1/2}/L_{avg} \tag{8}$$

or

$$n_I = \frac{2}{L_{avg}}\frac{(\lambda_A - \lambda_B)^{1/2}}{\lambda}\left(\frac{\Delta C}{\Delta X}\right)^{1/2}. \tag{9}$$

If the average length of the dislocations is related in some manner to a multiple $m$ of the average distance between dislocations, $n_A^{-1/2}$, we can set

$$L_{avg} = mn_A^{-1/2} = \frac{m\lambda}{(\lambda_A - \lambda_B)^{1/2}}\left(\frac{\Delta C}{\Delta X}\right)^{-1/2}. \tag{10}$$

It then follows that

$$n_I = \frac{2n_A}{m} = \frac{2}{m}\frac{(\lambda_A - \lambda_B)}{\lambda^2}\left(\frac{\Delta C}{\Delta X}\right). \tag{11}$$

### 2.4. Interactions Between Dislocations

We previously remarked that there are two sets of misfit dislocations in (100) planes, orthogonal to each other. Also, there is a third set of dislocations, the $n_I$ inclined dislocations, which lies roughly orthogonally to the other two sets. The possible interactions that might occur between the sets, of dislocations are important in interpreting the transmission electron micrographs to be shown later.

There are two possible types of misfit dislocations, pure-edge and mixed. We consider that the axes of both the pure-edge and mixed misfit dislocations are parallel to either the [011] or [01$\bar{1}$] directions. The difference between them is that the Burgers vector of the pure-edge lies in the (100) growth phase and is normal to the axis of the dislocation; the Burgers vector of the mixed misfit is inclined at 45° to the (100) plane and is not normal to the axis of the dislocation.

The pure-edge dislocations are twice as effective in relieving the mismatch strain, but the mixed dislocations will still form. In fact, observations shown later will indicate that they are present in roughly equal amounts.

We consider here misfit dislocations in only the (100) plane, since this was the plane of growth in these studies. Consideration of a different low index plane, such as the (111), would lead to different results in detail, but not in principle. The controlling feature here is the possible reduction in elastic energy that is produced when two dislocations interact. If combination of the Burgers vectors leads to an increase in elastic energy, no reaction will occur; this happens when $\mathbf{b}_1^2 + \mathbf{b}_2^2 < \mathbf{b}_3^2$, where $\mathbf{b}_1$ and $\mathbf{b}_2$ are the magnitudes of the Burgers vectors of the reactant dislocations and $\mathbf{b}_3$ is the corresponding quantity for the product dislocation.

The possible interactions can be reduced to three, as shown schematically in fig. 3 for the (100) plane. The left column indicates the Burgers vectors of the reactant dislocations while the right column indicates the configurations and

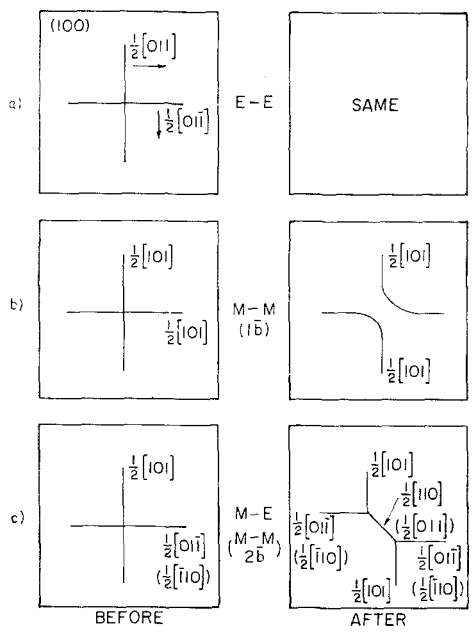


*Figure 3* Schematic representation of interactions between misfit dislocations lying in (100) misfit plane.

Burgers vectors of the product dislocations. The letters between the columns indicate the types of reactant dislocations being considered: E = pure-edge and M = mixed dislocation.

In fig. 3a, we see that no reaction is expected between orthogonal pure-edge dislocations; this is because no force is developed at the crossing point.* In fig. 3b, we consider the case of two mixed dislocations, each having the same Burgers vector. Reaction between these occurs so as to eliminate the crossing point and, thus, reduce the line energy of the dislocations. In fig. 3c, two reactions are considered, each of which lower the elastic energy of the system. The first reaction is that between a mixed and a pure-edge dislocation; the second reaction is between two mixed dislocations with different Burgers vectors, where we have put parentheses around both the Burgers vector of the horizontal mixed dislocation and the inclined product dislocation. In each of these cases, triple nodes are produced. If different Burgers vectors are chosen, the numbers will change, but the result will always be in the forms shown.

We next consider the interactions between the inclined dislocations $n_I$ and the misfit dislocations. It can be shown that these also reduce to three simple cases, similar to those shown in fig. 3, but differing in that one of the dislocations is an inclined dislocation. Actually, the inclined dislocations might be at an angle of 30° to the misfit dislocations, but since the Burgers vectors are of the same form, $(a/2) <110>$, as the misfit dislocations shown, the types of reactions occurring will be the same as indicated.

## 3. Experiments on $GaAs_{1-x}P_x$

### 3.1. Experimental Procedure

#### *3.1.1. Crystal Growth*

The epitaxial layers were prepared by Dr J. J. Tietjen using vapour phase growth [16] on the. $(\bar{1}00)$ plane of single crystal GaAs substrates The substrates had dislocation densities from $10^4$ to $10^5$ cm$^{-2}$ intersecting the $(\bar{1}00)$ plane; the dislocation density was evaluated by chemical etching [11]. Prior to growth, the substrates were chemically polished to remove surface damage.

The composition of the epitaxial layer was changed during growth from GaAs to $GaAs_{1-x}P_x$ by decreasing the flow of arsine in the vapour streams while increasing that of phosphine. Electron beam microprobe analysis showed that compositional gradient, $\Delta C/\Delta X$, was constant throughout the thickness of all the graded samples used in these experiments. The compositional gradient is measured here as the change in the mole per cent of phosphorus in the solid divided by the distance. In addition, one of the graded layers, $((\Delta C/\Delta X) = 5.0\%$ P/$\mu$m), was doped with Se ($n = 1.5 \times 10^{18}$ cm$^{-3}$), the doping being done directly in the vapour phase [16]. A total of six crystals were grown for these studies, including two control specimens of undoped expitaxial GaAs.

#### *3.1.2. Specimen Preparation*

A total of eleven specimens for transmission electron microscopy were prepared from 3.1 mm diameter discs ultrasonically cut from the epitaxially grown layers; the axes of the discs were parallel to the [100] direction. The discs were then carefully reduced to a thickness of 0.0025 cm using a solution of bromine in methanol. The final thinning of the specimens was performed by ion bombardment using $Ar^+$ ions; an ion beam current equal to 100 $\mu$A and potential of 6 kV were employed in a modified

*The reaction, $\frac{a}{2}[011] + \frac{a}{2}[01\bar{1}] \rightarrow a[010]$, might be expected to occur, but it has not been observed in this study (see [14, 15]).

ALBA ion bombardment machine* [17]. Cross-sectional (0 1 1) specimens were also prepared by cleaving sections from the epitaxial layers and proceeding in the above manner.

### 3.1.3. Electron Microscopy

An RCA EMU-3G electron microscope, operating at 100 kV and equipped with a tilting specimen holder, was used in this study. Stereo-pairs were obtained in the manner of Levine *et al* [18] by taking two exposures both before and after tilting the specimens approximately 8° about the normal to the $\{hkl\}$ planes. Kikuchi bands were used to maintain the same two-beam conditions. All the transmission electron micrographs shown here were taken in the two-beam bright field condition with $s = 0$, with the exception of fig. 6b, where three beams were employed.

Over twenty different areas were examined in each of the eleven different specimens, to guarantee that a true sampling was being made.

### 3.1.4. Dislocation Density Measurements

The density $n_A$, which is defined as the number of misfit dislocations/cm$^2$ emerging from the $<0\,1\,1>$ side faces of the crystal, was evaluated by using a 20 × 20 cm photographic print, of the type reproduced in fig. 4, typically corresponding to an overall magnification of about $10^4$ times. The number of intersections of dislocations with a line perpendicular to one of the two sets of misfit dislocations was recorded. Ten such measurements at different positions on the photograph were made for the same set of dislocations, and this process was repeated for the other perpendicular set of dislocations. Photographs of the same sample for different **g** were examined to insure that no dislocations were overlooked. The mean number of intersections as well as the standard deviation, were then determined and corrected for magnification. The quantity $n_A$ was evaluated by dividing the mean number by the sample thickness. In turn, for each sample, about ten different areas were then examined for the overall evaluation of $n_A$. We found no significant difference in the values of $n_A$ obtained from the set of misfit dislocations parallel to [0 1 1] and that set parallel to the [0 1 $\bar{1}$] direction. In general, the standard deviations for the values of $n_A$ reported below are about ± 20%.

The values of $n_I$ were obtained from the same type of photographic print. The number of inclined dislocations was counted, divided by the area of the print, and corrected for magnification. Care was taken to avoid overlooking any inclined dislocations, and also to take into account the fact that inclined dislocations can terminate at both foil surfaces. Again, about ten different areas on a given sample were used to evaluate $n_I$. The standard deviations of the $n_I$ are about ± 30%.

## 3.2. General Observations

### 3.2.1. Three-Dimensional Network

In fig. 4, misfit dislocations are seen in a graded layer and are largely parallel to the [0 1 1] and [0 1 $\bar{1}$] directions. Thus, when viewed parallel to the [1 0 0] direction, they form parts of a square grid similar to fig. 1, except that dislocations are connected and stereoscopic examination reveals that the dislocations are arranged in the form of a three-dimensional network. Many of the dislocations parallel to [0 1 1] and [0 1 $\bar{1}$] in fig. 4 are closely spaced; stereoscopic examination in similar regions has revealed that in general they are spread out through the sample thickness. Virtually all of them bend out of the plane, thus giving rise to inclined dislocations, and this corroborates one of the major postulates of the model.

Specimens from an undoped epitaxial GaAs layer grown on an undoped (1 0 0) GaAs substrate were also examined. The specimens were obtained from near the middle of the 20 μm thick epitaxial layer. They were found to be featureless, except that on occasion inclined dislocations were observed with a density too low to be evaluated, the lower limit of detection being about $10^5$ cm$^{-2}$.

### 3.2.2. Burgers Vectors

The misfit dislocations are shown in fig 4 for the reciprocal lattice vectors, **g**: $0\,2\,\bar{2}$, $0\,\bar{2}\,\bar{2}$, $0\,\bar{4}\,0$, $0\,0\,\bar{4}$. Representative examples of the contrast which occurs are seen near the numeral 1. The dislocation beneath the numeral 1, which is parallel to [0 1 $\bar{1}$] vanishes for $\mathbf{g}_{02\bar{2}}$. By application of the $\mathbf{g}\cdot\mathbf{b} = 0$ criterion for the invisibility of a dislocation, where **b** is the Burgers vector of the dislocation, it is seen that **b** is parallel to [0 1 1]. Thus, this dislocation is of the pure-edge type with $\mathbf{b} = (a/2)$ [0 1 1], making the usual assumption that **b** corresponds to the shortest transla-

*ALBA Ion Bombardment Machine, developed by Professor Paulus, CNRS, Bellevue, France, and marketed by ALBA Engineers, Asnières, France.

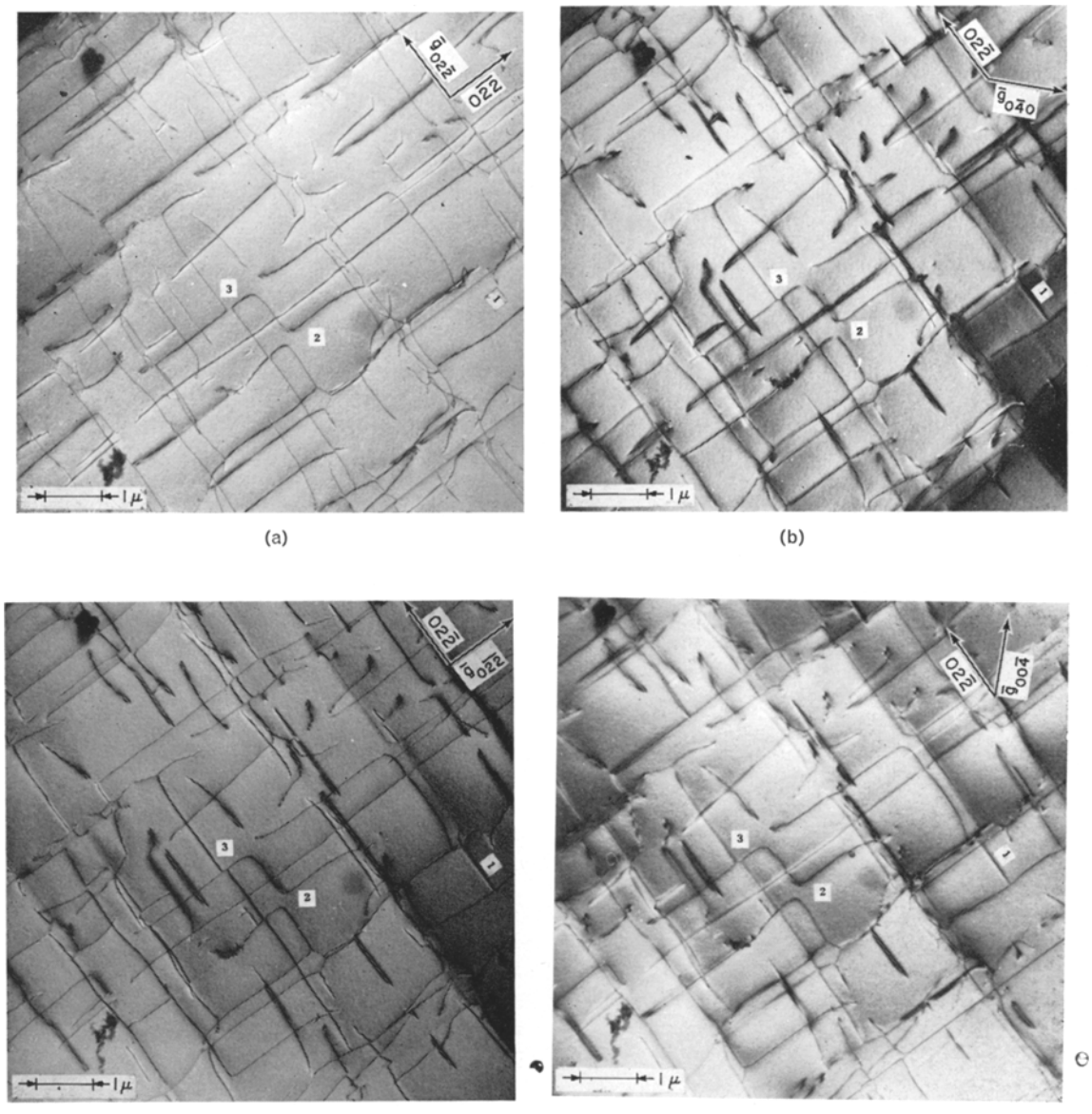


*Figure 4* Dislocation network in compositionally graded layer: (a) $\mathbf{g}_{02\bar{2}}$; (b) $\mathbf{g}_{0\bar{2}2}$; (c) $\mathbf{g}_{0\bar{4}0}$; (d) $\mathbf{g}_{00\bar{4}}$. (100) foil orientation.

tion vector in the sphalerite structure. By similar reasoning, the dislocation to the left of the numeral 1 is also pure-edge, but with $\mathbf{b} = (a/2)[01\bar{1}]$, where $a$ is the lattice constant. These edge dislocations with **b** parallel to the (100) growth interface are expected since they provide the most efficient strain relief [19].

In addition to these pure-edge misfit dislocations, there are also present misfit dislocations whose Burgers vectors lie along the <110> directions that are inclined at 45° to the (100) plane. These mixed misfit dislocations have an efficiency of strain relief equal to one-half that of the pure-edge [19]. Fig. 5 shows (for $\mathbf{g}_{00\bar{1}}$ and $\mathbf{g}_{0\bar{4}0}$) a typical nodal reaction (adjacent to the numeral 1) between two misfit dislocations each having an inclined Burgers vector. It is seen in fig. 5 that only some portions of the dislocations are invisible. This is due to two effects. Firstly, the dislocations are not straight and probably do not lie totally in the ($\bar{1}$00) plane which indicates that the sufficient condition for invisibility,

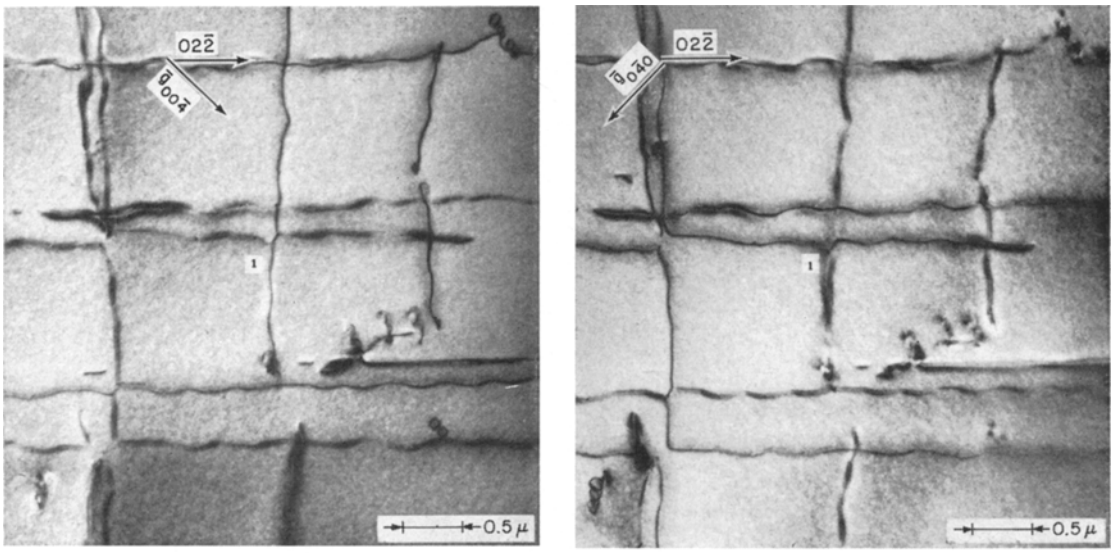


*Figure 5* Dislocation network in compositionally graded layer: (a) $\mathbf{g}_{00\bar{4}}$; (b) $\mathbf{g}_{0\bar{4}0}$. (100) foil orientation. This is a different area in the same specimen as in fig. 4.

$\mathbf{g}\,\mathbf{b} \times \mathbf{u} = 0$, where $\mathbf{u}$ is a unit vector tangent to the dislocation, cannot be achieved at all parts of the dislocation. Secondly, the dislocations were observed to be decorated, at least in part. Decorating particles can be seen along portions of the lower two horizontal dislocations in fig. 5b. The Burgers vectors have been evaluated by application of the $\mathbf{g}\,\mathbf{b} = 0$ rule to those parts of the lines which *do* go out of contrast. This determination of $\mathbf{b}$ is valid for uninterrupted portions of the same dislocation, since $\mathbf{b}$ must be constant along a dislocation. The horizontal dislocation has $\mathbf{b} = (a/2)\ [110]$ (or $(a/2)\ [\bar{1}10]$), while the vertical dislocation has $\mathbf{b} = (a/2)\ [\bar{1}01]$ (or $(a/2)\ [101]$). The dislocations were totally in contrast for $\mathbf{g}_{02\bar{2}}$ and $\mathbf{g}_{0\bar{2}2}$ which are not reproduced here.

It should be noted that these two types of Burgers vectors (i.e. either lying in or inclined at 45° to the plane of growth) were the only ones associated with total dislocations in this study. Both types were observed in all the graded layers.

### *3.2.3. Sign of the Dislocations*

If the dislocations in the (100) planes are of the misfit type, they should all have the same sign (i.e. the extra half-planes of the dislocations should all be oriented the same way). It was determined that this is the case for the misfit dislocations in each of the linear grids. For example, fig. 6a shows that the discontinuous change in contrast that occurs across each dislocation is almost always in the same dark-to-light sense. This indicates that the local bending of the foil is in the same sense for each dislocation [20], indicating that they all have the same sign. Another example which shows double images of the dislocations parallel to the [011] direction is shown in fig. 6b. Here, both $\mathbf{g}_{00\bar{4}}$ and $\mathbf{g}_{022}$ were used to form the image. It is seen that the weaker of the two images is consistently to the left of the stronger image, which again indicates that the dislocations are of the same sign [21].

## 3.3. Dislocation Interactions

It was previously suggested that misfit dislocations eventually bend out of the plane to form inclined dislocations. However, because of dislocation interactions, they can also appear to bend within the misfit plane.

Before discussing dislocation interactions, it must be pointed out that there are two types of dislocations to be distinguished in the electron micrographs of (100) foils. These are the misfit dislocations lying parallel to the (100) plane, and the inclined dislocations lying at an angle to the (100) plane. The foil thicknesses used here are about 0.1 $\mu$m and, thus, a dislocation whose projected length on (100) is greater than about 1 $\mu$m lies effectively parallel to the (100) plane. On the other hand, a dislocation segment whose projected length is less than about $1/2\mu$m is

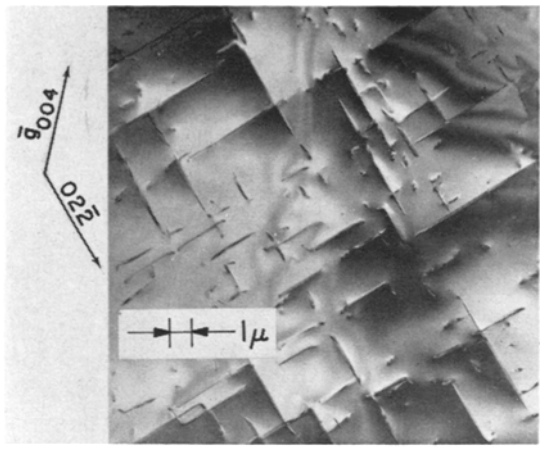


(a)

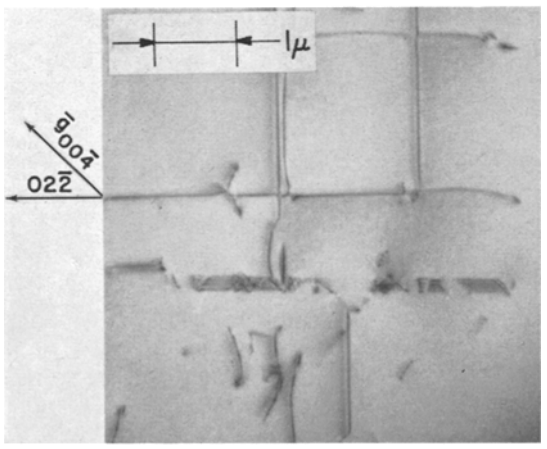


(b)

*Figure 6* Dislocation network in compositionally graded layer, showing in (a) discontinuous change in contrast across dislocations ($\mathbf{g}_{004}$) and (b) double images of dislocations ($\mathbf{g}_{00\bar{4}}$ and $\mathbf{g}_{022}$); (100) foil orientation. This is a different area in the same specimen as in figs. 4 and 5.

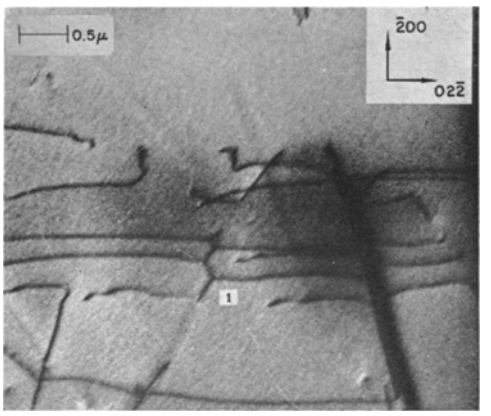


*Figure 7* Misfit and inclined dislocations in compositionally graded layer; $\mathbf{g} = \bar{3}1\bar{1}$, (011) foil orientation. Note that growth direction is vertical. The phosphorus composition was varied from 0 to 50% over a distance of 38 μm.

inclined to the (100) plane. In general, steeply inclined dislocations are recognized by their zig-zag contrast on the electron micrographs.

We now turn to the interactions shown in fig. 3b and 3c. Examples of these reactions between misfit dislocations are shown, respectively, in fig. 4 near the numerals 2 and 3. Many other examples of these exist in other places in the same micrograph. Also, the misfit dislocations can interact with inclined dislocations as seen clearly in fig. 7, which is an (011) foil obtained by thinning a cross-sectional sample formed by cleaving, for which $(\Delta C/\Delta X) = 1.3\%$ P/μm. In fig. 7, the growth direction is vertical and the horizontal dislocations are misfit dislocations. Near the numeral 1, we see an example of successive reactions corresponding to that depicted in fig. 3c. Here, the misfit dislocations with Burgers vector $\mathbf{b}_1$ have been intersected by and reacted with an inclined dislocation with $\mathbf{b}_2$ to form short product dislocations with $\mathbf{b}_3$. Moreover bending of the misfit dislocations out of the $[01\bar{1}]$ direction can be seen in fig. 7.

A possible example of two intersecting non-interacting dislocations, corresponding to fig. 3a, is shown in fig. 4 near the numeral 1. It was previously shown (section 3.2.3.) that these two dislocations are, indeed, pure-edge dislocations. However, we cannot distinguish between intersecting, non-interacting dislocations as compared to two non-intersecting dislocations in different planes. Nevertheless, from the frequency with which we have observed dislocations crossing without apparent interactions, it appears exceedingly likely that some of these "crossings" are bona-fide "intersections without interaction".

Thus, the classification of dislocations as either misfit or inclined, and the classification of dislocation interactions into the three types shown in fig. 3, allows an excellent interpretation of the dislocation morphology revealed by the transmission electron micrographs. This presents a general and fairly complete cataloguing of misfit dislocation networks due to composition changes or gradients.

### 3.4. Dislocation Density in Compositionally Graded Layers

The densities $n_A$ and $n_I$ are given in equation 6 and 11 as a function of the compositional gradient. It is noteworthy that there are no adjustable parameters in equation 6, while the quantity $m$ is the only adjustable parameter in equation 11.

The qualitative variation of $n_A$ is shown in fig. 8 for a wide range of compositional gradients. In fig. 9 we have plotted the experimentally determined mean values of $n_A$ versus $(\Delta C/\Delta X)$. It can be seen that the expected linear relation in equation 6 holds. Next, it would be expected that the value of $n_A$ is independent of its position in the crystal, i.e. independent of the distance of the sample from the substrate. That this is true is shown in fig. 10, where $n_A$ $(\Delta C/\Delta X)^{-1}$ is plotted against $\Delta X$.

Concerning quantitative agreement with equation 6, we note that $\lambda$ must be resolved into its component in the $<110>$ direction which is

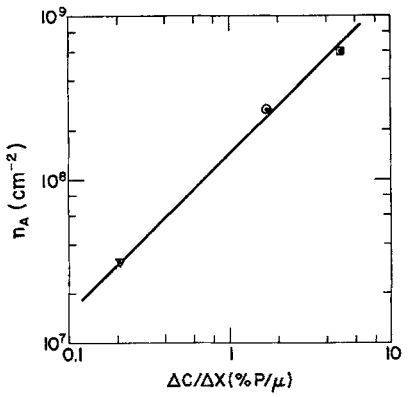


*Figure 9* Dependence of mean values of $n_A$ on $(\Delta C/\Delta X)$.

equal to $a/\sqrt{2}$ where $a$ is the lattice constant. From Tietjen and Amick [16], we find that $a = 5.6$ Å for this range of compositions, and changes by a value of 0.002 Å for a change of 1 % phosphorus. If the dislocations are all pure-edge, the value of $n_A$ is predicted to be $8.8 \times 10^7$ cm$^{-2}$

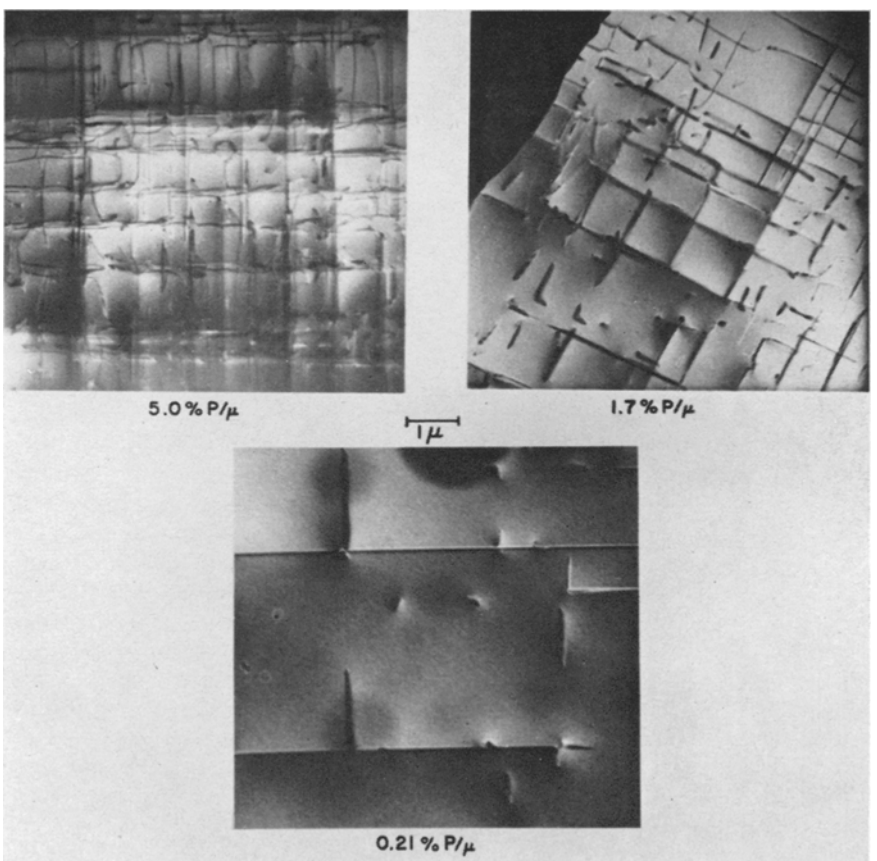


*Figure 8* Misfit dislocation network at the middle of three crystals grown with three different values of $(\Delta C/\Delta X)$.

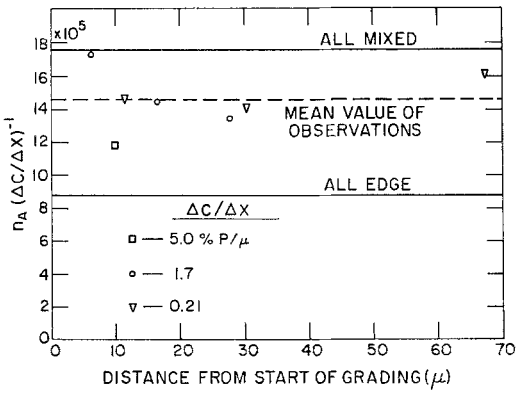


*Figure 10* Plot of $n_A/(\Delta C/\Delta X)$ vs. distance from the start of compositional grading. The solid lines indicate the values for this parameter if all dislocations were either pure-edge or else mixed.

for a composition gradient of 1% P/$\mu$m. If they are all mixed, the value of $n_A$ should be twice as much, $1.7 \times 10^8$ cm$^{-2}$, since the strain relieving efficiency of the mixed type is only one half that of the pure-edge. It can be seen from fig. 9 that the observed values of $n_A$ at 1% P/$\mu$m is in excellent agreement with the theory. Furthermore the expected densities for all the observations are indicated in fig. 10. We see that the data points fall between the two calculated limits of all pure-edge and all mixed. The dashed line, representing the mean value of the observations, indicates that the misfit dislocations are neither all pure-edge nor all mixed, but rather a combination of both types.

Next, according to equation 10, the average length of a dislocation should vary inversely with $(\Delta C/\Delta X)^{1/2}$. This relationship is shown in fig. 11,

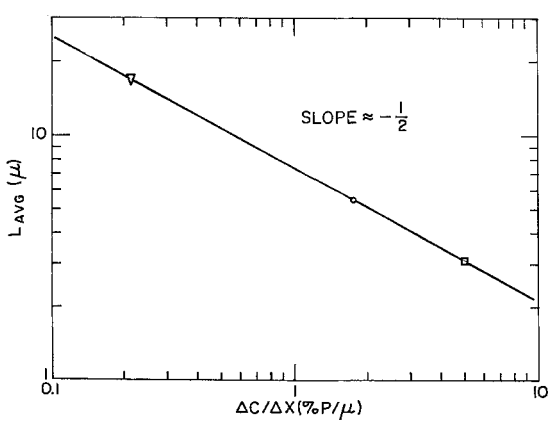


*Figure 11* Dependence of average segmented dislocation length, $L_{avg}$, on $n_A$.

where the average length is determined from the full length of the dislocations, whether or not they bend back and forth within the plane. From the slope of fig. 11, it is derived that the average length of such segments is roughly eight times the average distance between dislocations. That equation 10 holds, implies that indeed, the average dislocation length is related to the dislocation density.

According to equation 11, qualitatively $n_I$ should vary linearly with $(\Delta C/\Delta X)$. We test this relation in fig. 12, where the mean values of $n_I$ have been plotted as a function of $(\Delta C/\Delta X)$ on log-log paper. The data define a straight line which has a slope slightly greater than unity. Thus, the expected relationship between $n_I$ and $(\Delta C/\Delta X)$ is generally borne out.

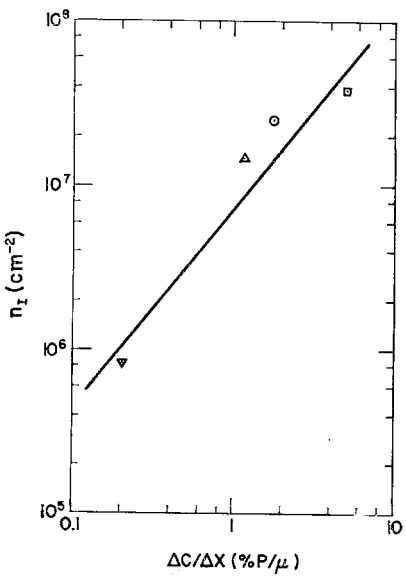


*Figure 12* Variation of mean values of $n_I$ with $(\Delta C/\Delta X)$.

We now quantitatively compare the data with equation 11. At 1% P/$\mu$m $n_A = 1.4 \times 10^8$ cm$^{-2}$ (see fig. 9). Since $m = 8$, $n_I$ is predicted to be $3.5 \times 10^7$ cm$^{-2}$. In fig. 12, it is found that $n_I = 1\text{–}2 \times 10^7$ cm$^{-2}$, which is in reasonable agreement with the predicted value.

One of the main postulates of the model in section 2.2. is that the value of $n_I$ remains constant during growth. The validity of the assumption is illustrated in fig. 13 for two values of compositional gradient. It can be seen that the value of $n_I$ remains constant within experimental

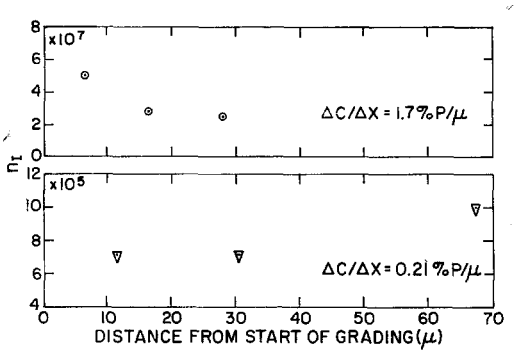


*Figure 13* Dependence of $n_I$ on sample position $\Delta X$ for two compositional gradients.

error, and independent of the site of removal of the specimen from the graded heterojunction.

Further corroboration for the constancy of $n_I$ with growth distance was provided from a study of the variation of $n_I$ with specimen thickness. It was found that for specimens ranging from 0.14 $\mu$m to 0.36 $\mu$m thick, no systematic variation of $n_I$ could be discerned.

We also note that the linear relation between $n_A$ and $n_I$, (see equation 11), has been found. Although the graph is not shown here, this linear relation follows from the results presented in figs. 9 and 12.

### 3.5. Dislocations in Constant Composition Layers

We present here results obtained on the dislocation morphology in a layer of constant composition, which is grown on a graded layer. In particular, a 75 $\mu$m thick layer of $GaAs_{0.55}P_{0.45}$ was grown on top of a graded layer for which $(\Delta C/\Delta X) = 1.1\%$ P/$\mu$m. Both the constant composition and graded layers were undoped.

Transmission electron micrographs, obtained from the top and bottom of the constant composition layer, are shown in fig. 14, where the plane of observation is (100). We note first, that there are no misfit dislocations present (compare with fig. 5). We note secondly, however, that there are inclined dislocations present and that their density, equal to $1.4 \times 10^7$ cm$^{-2}$, is the same at the top as at the bottom.

These results agree with our expectations. No misfit dislocations are present because $(\Delta C/\Delta X) = 0$ in this layer. On the other hand, it is expected that the $n_I$ inclined dislocations produced in the compositionally graded layer will propagate into and through the constant composition layer. This occurs because there is no mechanism available for their elimination. They cannot reach the sides of the crystal since the ratio of width to thickness of the grown layer is large.

## 4. Conclusions

Both a theoretical and experimental study has provided a simple model for the dislocation morphology at a heterojunction. Formation of a heterojunction, whether abrupt or graded, gives

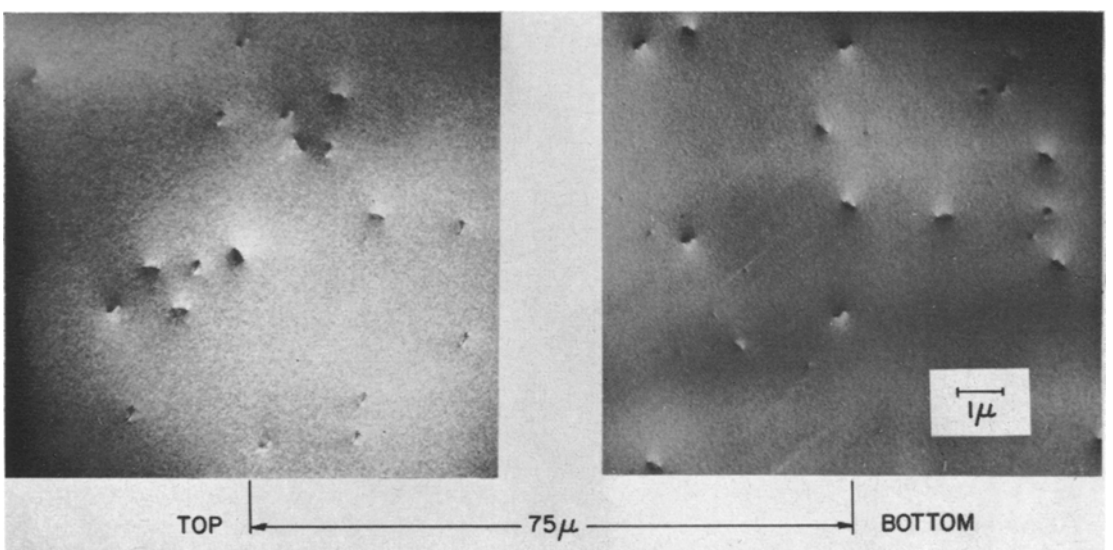


*Figure 14* Inclined dislocations at top and bottom of 75 $\mu$m thick constant composition layer grown on a graded heterojunction.

rise to not only a set of misfit dislocations lying in the plane of growth, but also a set of inclined dislocations, $n_I$, which propagate throughout the growing crystals. This occurs because the misfit dislocations are segmented, and since they cannot end within the crystal, must bend upwards into the plane of growth. The value of $n_I$ remains constant throughout the crystal, since no additional misfit dislocations are formed because the inclined dislocations can bend in and out of subsequently formed misfit planes.

It is found that these inclined dislocations will propagate through an ungraded region grown onto a graded heterojunction and this is of importance in device fabrication. Thus, to decrease the value of $n_I$, the compositional grading at the heterojunction must be decreased, since it is not sufficient to merely grow additional material at constant composition. In the $GaAs_{1-x}P_x$ system, the value of $n_I$ decreases from $4 \times 10^7$ cm$^{-2}$ to $10^6$ cm$^{-2}$ with a decrease in compositional gradient from 5% P/$\mu$m to 0.2% P/$\mu$m. It is also seen that the dislocation densities can be quite high, orders of magnitude higher than the densities in the substrates.

Finally, the data indicate that the misfit dislocations are a combination of pure-edge and mixed. This affects the interaction that occurs when two misfit dislocations cross, and cause the dislocations to appear to bend back and forth in the plane. Three possible cases are (1) no interaction occurs, (2) interaction eliminates the intersection, (3) a triple node is formed. All three cases are found to occur.

## Acknowledgements

The authors are particularly grateful to Dr J. J. Tietjen and Mr H. Gossenberger for supplying the vapour grown $GaAs_{1-x}P_x$ samples, without which this work could not have been performed.

## References

1. R. L. ANDERSON, *Solid-State Electron* **5** (1962) 341.
2. H. KROMER, *Proc. IRE* **45** (1957) 1537.
3. D. A. JENNY, *ibid* **46** (1958) 959.
4. J. J. TIETJEN *et al*, *Trans. AIME* **239** (1967) 385.
5. C. J. NUESE *et al*, *ibid* **242** (1968) 400.
6. R. E. ENSTROM, to be published.
7. D. RICHMAN and J. J. TIETJEN, *Trans. AIME* **239** (1967) 418.
8. F. C. FRANK and J. H. VAN DER MERWE, *Proc. Roy. Soc.* **A198** (1949) 216.
9. M. S. ABRAHAMS and C. J. BUIOCCHI, *J. Appl. Phys.* **37** (1966) 1973.
10. R. S. MROCZKOWSKI, A. F. WITT, and H. C. GATOS, *J. Electrochem. Soc.* **115** (1968) 750.
11. M. S. ABRAHAMS and C. J. BUIOCCHI, *J. Appl. Phys.* **36** (1965) 2855.
12. J. H. VAN DER MERWE, *ibid* **34** (1963) 117; **34** (1963) 123.
13. W. A. JESSER and D. KUHLMANN-WILSDORF, *Phys. Status Solidi.* **19** (1967) 95.
14. F. C. FRANK "Defects in Crystalline Solids" (The Physical Society, London, 1955) p. 166.
15. J. W. MATTHEWS "Single Crystal Films", edited by M. H. Francombe and H. Sato (The MacMillan Co, New York, 1964) p. 167.
16. J. J. TIETJEN and J. A. AMICK, *J. Electrochem. Soc.* **113** (1966) 724.
17. M. S. ABRAHAMS, C. J. BUIOCCHI, and M. D. COUTTS, *Rev. Sci. Instr.* **39** (1968) 1944.
18. E. LEVINE, J. WASHBURN, and G. THOMAS, *J. Appl. Phys.* **38** (1967) 81.
19. J. W. MATTHEWS and W. A. JESSER, *Acta Met.* **15** (1967) 595.
20. R. SIEMS, P. DELAVIGNETTE, and S. AMELINCKX, *Phys. Status Solidi.* **2** (1962) 421.
21. P. B. HIRSCH, A. HOWIE, and M. J. WHELAN, *Phil. Trans. Roy. Soc.* **A252** (1960) 499.